Charge trapping defects in CdSe nanocrystal quantum dots

Antonio J. Almeida,[†] Ayaskanta Sahu,[‡] Andreas Riedinger,[‡] David J. Norris,[‡]
Martin S. Brandt,[¶] Martin Stutzmann,[¶] and Rui N. Pereira[*,†,¶]

Department of Physics and I3N, University of Aveiro, Campus Universitário de Santiago, 3810-193 Aveiro, Portugal, Optical Materials Engineering Laboratory, ETH Zurich, 8092 Zurich, Switzerland, and Walter Schottky Institut and Physik-Department, Technische Universität München, Am Coulombwall 4, 85748 Garching, Germany

E-mail: rnpereira@ua.pt

Abstract

Charge trapping due to defects in semiconductor quantum dots (QDs) is expected to challenge the applicability of QDs in future technologies. The efficient elimination of defects from QDs demands an understanding of their origin and of their impact on (photo)electronic properties. Here, we identify the presence of two charge states of a defect in CdSe QDs using electron paramagnetic resonance, combined with electronic tuning of QDs via chemically induced Ag doping. From light-induced EPR, we show that these defects have a central role on Fermi level pinning in QD ensembles. By analyzing the dependence of the EPR signal of the defects on the concentration of Ag dopants, we further demonstrate that the defects act as effective electron traps in

---

[*] To whom correspondence should be addressed
[†] University of Aveiro
[‡] ETH Zurich
[¶] Technische Universität München

the QDs. Our study also provides support to the proposed behavior of Ag dopants in CdSe QDs, according to which Ag atoms are n-type dopants at concentrations below 2 Ag atoms per QD and become p-type dopants for higher Ag concentrations. From temperature dependent EPR, we estimate a lower limit for the ionization energy of the studied defects. Based on the characteristics of the EPR spectrum, we propose that these defects are associated to Se vacancies with the paramagnetic state being the positively charged state of the defect.

Introduction

Semiconductor nanocrystal quantum dots (QDs) are crystallites of semiconductor materials only a few nanometers in size that display a wealth of remarkable properties arising from their small size. The properties of QDs include size-dependent band-gap[1] and photoluminescence,[2–4] multiple exciton generation,[3–7] and extremely high surface-to-volume ratio. These properties make semiconductor QDs promising as building blocks for a wide range of (opto)electronic applications. Of particular interest are metal-chalcogenide QDs, namely QDs made of CdX and PbX (X= S, Se, and Te), whose application in devices has enabled impressive performances. For example, light-emitting devices based on solution-processed semiconductor QDs have been demonstrated with a luminescence efficiency of up to 18% and a size-tunable emission color.[8] Metal-chalcogenide QDs have also proven suitable for use as light-absorbing materials in photovoltaics,[9–11] where devices based on ZnO/PbS core-shell QDs have achieved efficiencies near 8.5%.[12] Further, CdSe QDs have been used to fabricate thin-film field effect transistors (FETs) that can be incorporated in complex integrated devices.[13]

Defects are one of the main factors limiting the performance of QD-based devices.[14–27] Electrically active defects give rise to energy states energetically localized within the QD's energy gap that capture charge carriers from delocalized electronic states of the QDs.[23] The presence of trap states reduces the mobility and the diffusion length of charge carriers across films of QDs.[25] Trap states can also be centers of fast non-radiative recombination of photogenerated charge carriers.[17,24–27] Furthermore, recombination at trap states leads to a quenching of the QDs photoluminescence.[26] A wealth of studies has demonstrated the negative impact of charge traps on the performance of QD-based photovoltaic devices.[14,17,25,26,28] For example, some studies showed that the number and energy of trap states in QDs lead to a reduction of the open circuit voltage and the short circuit current of solar cells.[14,17,28] Other studies have shown that charge traps acting as recombination centers limit the photocurrent extraction from QD-based solar cells.[25]

To develop new strategies for the elimination of trap states from QD-based devices and thus improve their performance, it is crucial to identify the defects responsible for these states and to further understand their impact on electronic properties. However, there have been only a few attempts to identify the origin of charge traps in metal-chalcogenide QDs, both experimentally[14–16,24,29] and theoretically.[24,30–32] Some of these studies have suggested the presence of charge traps at the QDs surface.[16,24,30,31] First-principle calculations of CdSe QDs have suggested that charge traps can result from incomplete passivation of the QDs surface.[24,30–32] Experimental support for these predictions was provided by photoelectron spectroscopy measurements of PbS QDs films, which showed that passivating the QDs surface with halide ligands leads to a reduction in the number of midgap trap states.[16] However, it has also been proposed that defects in the bulk of the QDs (bulk defects) may give rise to trap states,[14,15,29] regardless of the quality of the QD's surface passivation. In PbS QDs, trap states were suggested to originate from metal ions in the QD's bulk by comparing the trap capture cross section measured by thermal admittance and deep level transient spectroscopies with the ionic radius of metal ions.[14] Conductivity studies of CdSe/ZnS core/shell QDs observed trap states with an activation energy close to that of Se vacancies in bulk CdSe.[15] In CdS QDs, point defects have been observed by electron paramagnetic resonance (EPR) spectroscopy and assigned to S vacancies by comparison of their g-factor with that reported for S vacancies in bulk ZnS.[29] In spite of these advances, a definite identification of defects in metal-chalcogenide QDs has been elusive and their effect on the performance of devices based on these QDs has remained largely uncharted.

In this study, we experimentally identify charge trapping defects in CdSe QDs using EPR spectroscopy. We propose that these defects are associated to Se vacancies with the paramagnetic state being the positively charged state of the defect. From light-induced EPR, we demonstrate that the observed defects have a determinant role in pinning the Fermi level in QD ensembles. We further provide evidence for the previously proposed behavior of Ag dopants in CdSe QDs, according to which Ag dopants are *n*-type donors for concentrations below about 2 Ag atoms per QD (Ag/QD) and become *p*-type acceptors for higher Ag concentrations.[33]

Results and discussion

Transmission electron microscopy (TEM) images of undoped CdSe QDs show that these have a spherical shape and a narrow size distribution; see Fig. 1(a). Figure 1(d) shows the X-ray diffraction pattern of these QDs (black line) which can be matched to the wurtzite structure (JCPDS #08-0459) of CdSe. Further, the absorption spectra of the undoped CdSe QDs studied here, shown in Fig. 1(e) (black line) is similar to that previously reported for undoped CdSe QDs.[20,34,35]

The EPR spectrum measured at room temperature for a sample of undoped CdSe QDs powder sealed under nitrogen atmosphere is shown in Fig. 2 (black line). In the EPR spectrum we observe a signal centered at $g = 2.0045 \pm 0.0002$ with a peak-to-peak line width of about 0.8 mT. To obtain further information on the paramagnetic states that give rise to this signal, we performed photoexcited EPR measurements of our CdSe QDs. Figure 3 compares the EPR spectra measured at room temperature of a sample of undoped CdSe QDs powder sealed under nitrogen atmosphere measured in the dark (black line) and under white-light illumination (yellow line). We see that the EPR signal measured under illumination is about 3 times more intense than that measured in the dark. In the figure, we also see that the shape of the signal at $g = 2.0045$ observed under illumination is identical to that measured in the dark. We further observed that about 6 hours after ceasing illumination the intensity of the EPR signal returns to that initially measured in the dark, which indicates that the observed response to photoexcitation is reversible. This response to photoexcitation was observed for all CdSe QD powder samples analyzed in this study. The observed increase in the intensity of the EPR signal at $g = 2.0045$ under illumination indicates that photoexcitation leads to the generation of paramagnetic states in the CdSe QDs. This already demonstrates that these states should affect the kinetics of photogenerated charges, such as those involved in photovoltaic devices.

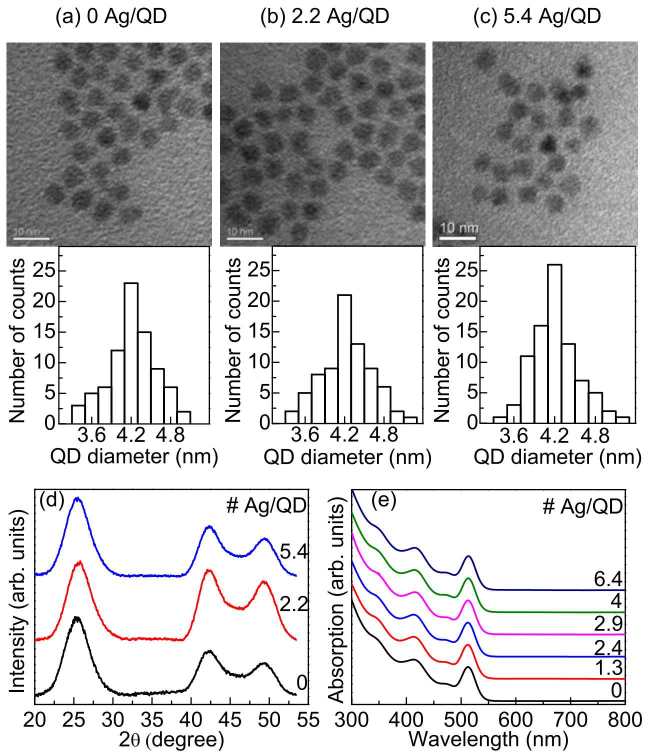

Figure 1: TEM images and QD size distributions of CdSe QDs (mean diameter of 4.2 nm): (a) undoped, (b) doped with 2.2 Ag atoms per QD (Ag/QD), and (c) doped with 5.4 Ag/QD. (d) X-ray diffraction spectra of the QDs shown in parts (a)−(c). (e) Absorption spectra for a series of CdSe QDs doped with different Ag concentrations (mean diameter of 2.7 nm).

Firstly, we discuss the origin for the paramagnetic states giving rise to the signal at $g = 2.0045$. Previous studies have identified paramagnetic defects in bulk II-VI semiconductors by EPR. In particular, these investigations have shown that singly charged anion vacancies give rise to sharp isotropic EPR lines near $g = 2$.[36–38] For example, positively charged S vacancies in ZnS were shown to yield an EPR signal at $g = 2.0034$ with a peak-to-peak line width of 0.05 mT by observing that this signal did not shift when the crystal was rotated around the axis of growth and by detecting the hyperfine structure of the first zinc shell around the anion vacancy.[36] In CdTe, positively charged Te vacancies were shown to yield an EPR signal with an isotropic g-value of $g = 2.000$ and peak-to-peak line width of 0.4 mT, based on the observation of the resolved isotropic hyperfine interaction of the vacancy with its four nearest Cd neighbors.[37] The assignments given in these investigations are unambiguous and, therefore, it is quite clear that positively charged anion vacancies in II-VI materials give rise to EPR signals with g-values close to g=2.00. There is an evident resemblance between the g-values reported in these studies and the value observed in the EPR spectra of our CdSe QDs. This suggests that the EPR signal at $g = 2.0045$ observed in our CdSe QDs is due to positively charged Se vacancies (V_{Se}^{+}) in the QDs. We note that the presence of these defects in CdSe has already been proposed previously.[15,39] We should emphasize that point defects (like vacancies) are very localized systems and the g-values are affected only by the close neighboring environment of the defect, which is similar in bulk and in QDs. Therefore, the g-values of vacancy defects should be identical in bulk and in QDs. In ZnSe, an EPR signal at $g = 2.0027$ with a peak-to-peak line width of 0.58 mT has also been attributed to positively charged Se vacancies,[38] based on the proximity of its g-value to that reported for positively charged anion vacancies in other II-VI materials.[36,37] Furthermore, a study on CdS QDs capped with poly(methyl 2-methylpropenoate) reported a slightly asymmetric line at $g = 2.004$ with a peak-to-peak line width of 1.5 mT.[29] This EPR signal was also attributed to positively charged S vacancies located at sites on the surface or near the surface of the QDs,[29] by comparison with the EPR signal reported for positively charged S vacancies in ZnS.[36] Although the proposed assignment of the defect observed in our EPR spectra of CdSe QDs to positively charged Se vacancies is not completely unambiguous, for the sake of simplicity we will use the label V_{Se}^{+} to refer to the defect giving rise to the observed EPR signal. Should the EPR signal originate from another defect the discussion below remains the same, but applied to the pertinent defect and corresponding charge states. We note that the EPR signal of the charge trapping defects studied here displays a quite symmetric line, which means that the defects are isotropic. Therefore, we conclude that the defects should be bulk defects, because surface defects are intrinsically anisotropic, which would result in an asymmetric EPR spectrum. This is expected from simple symmetry arguments and is also observed experimentally for defects in nanocrystals. For example, in the case of Si dangling bond defects in silicon nanocrystals, surface dangling bonds (anisotropic defects) result in a strongly asymmetric EPR spectrum, whereas bulk dangling bonds (isotropic defects) result in a symmetric EPR line.[40]

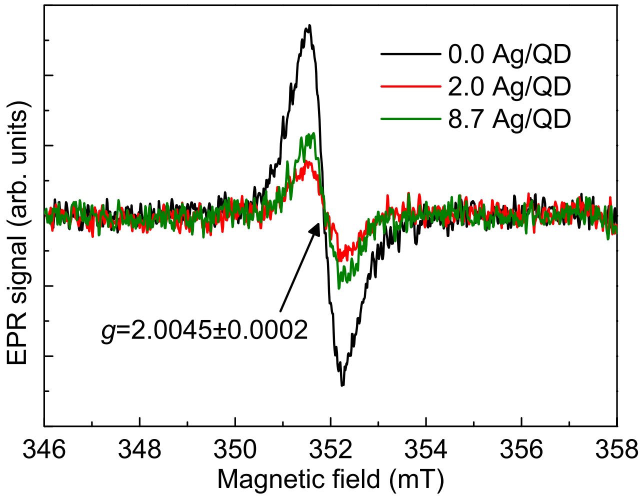

Figure 2: EPR spectra of undoped and Ag-doped CdSe QDs powder sealed under nitrogen atmosphere (mean diameter of 2.7 nm) measured in the dark at room temperature.

The EPR signal at $g = 2.0045$ is also observed in Ag-doped CdSe QDs, but its intensity depends on the concentration of Ag in the samples; see Fig. 2 (red and green lines). This observation indicates that the density of V_{Se}^{+} defects is affected by the amount of Ag dopants in the QDs. Figure 4 shows in more detail the dependence of the intensity of the EPR signal of V_{Se}^{+} defects on the concentration of Ag dopants as measured for two different sample batches. As can be seen, the intensity of the EPR signal at $g = 2.0045$ decreases with

Ag doping and reaches a minimum at $\sim$ 2 Ag dopants per QD (Ag/QD). Above this Ag concentration the intensity of the EPR signal increases with the Ag concentration.

To understand our data, we need to clarify the impact of Ag doping on the properties of the CdSe QDs. From TEM images, recorded for undoped and Ag-doped CdSe QDs, and QD size distributions obtained from such images [see examples in Figs. 1(a)−(c)], we can see that there are no significant changes in the mean size or size distribution of the QDs with doping. From the X-ray diffraction patterns obtained for the same QDs, shown in Fig. 1(d), we may see that the crystal structure of the QDs remains unchanged upon doping. Further, the absorption spectra of CdSe QDs shows that the energy band gap and optical absorption spectra remain unchanged after Ag doping; see Fig. 1(e). We should note that in a recent work carried out using X-ray absorption near-edge structure data combined with *ab-initio* simulations it was confirmed that the Ag dopants are incorporated inside our CdSe QDs.[41] In a previous study, Sahu *et al.* observed that the band-edge peak intensity of the fluorescence of Ag-doped CdSe QDs and the electron mobility of films of these QDs were maximum for Ag concentrations of about 2 Ag/QD.[33] These observations were associated to a change in the doping behavior with the concentration of Ag dopants in the QDs. For Ag concentrations up to $\sim$2 Ag/QD, Ag was proposed to be incorporated on interstitial sites of the QDs and behave as an n-type dopant.[33] For higher Ag concentrations, it was proposed that the dopants become incorporated on substitutional sites of the QDs and behave as p-type dopants.[33] This behavior of Ag dopants in CdSe QDs is supported by the trend observed by us for the variation of the intensity of the EPR signal of paramagnetic defects with the concentration of Ag dopants.

From the analysis of this trend, we may understand the charge trapping mechanism involving the paramagnetic defects in the CdSe QDs. For simplicity, the discussion presented here is made for the situation where the paramagnetic defect observed in EPR corresponds to $\mathrm{V}_{\mathrm{Se}}^{+}$. As described above, we observe a 3-fold increase in the intensity of the EPR signal of paramagnetic defects upon photoexcitation, as shown in Fig. 3. This observation indicates

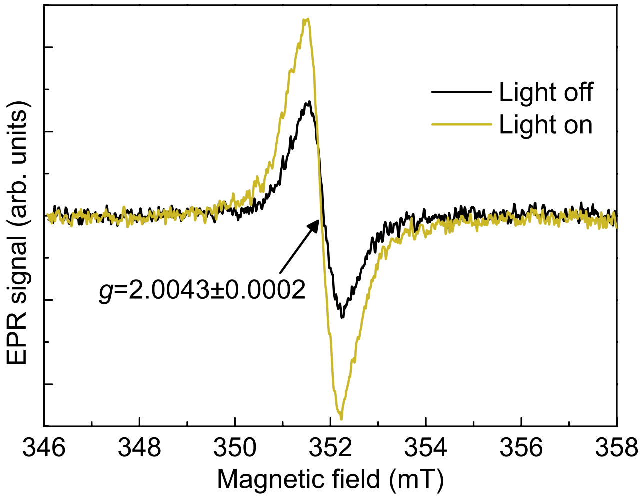

Figure 3: Comparison between EPR spectra of CdSe QDs (undoped) powder sealed under nitrogen atmosphere measured at room temperature, in the dark (black line) and under white light illumination (yellow line).

that in the dark there are two charge states of the defects present in the QD ensemble, i.e. the positive charge state (observed by EPR) and another charge state that is not observed by EPR (EPR-silent charge state). Moreover, we can conclude that the amount of defects in each of the two charge states is comparable. From this, we infer that the Fermi energy E_F of the QD ensemble is determined by the populations of the two charge states of the defect (Fermi level pinning). Previous investigations of charge transport of field effect transistors (FET) made with undoped CdSe QDs similar to those used in this work have concluded that the FETs exhibit n-type behavior.[33] Therefore, the Fermi energy in ensembles of undoped QDs should be located closer to the conduction band (CB) edge than to the valance band (VB) edge. This indicates that the EPR-silent charge state of the defect should be neutral. In this situation, the Fermi level in the QD ensemble is then determined by the $\mathrm{V}_\mathrm{Se}^{0/+}$ energy levels of the defects present in the QDs. Here, we consider that the defects are randomly placed in the different QDs of the ensemble and that there are differences in the $\mathrm{V}_\mathrm{Se}^{0/+}$ level of the different defects depending on their specific location within the QD. In practice, this corresponds to a distribution of $\mathrm{V}_\mathrm{Se}^{0/+}$ levels in the ensemble. We describe this distribution with a gaussian function having a maximum at an energy E_d, as shown in Fig. 5(a) for the case of undoped QDs. In this figure, the filled (red) area in the distribution of $V_{\mathrm{Se}}^{0/+}$ energies represents the amount of defects in the neutral charge state (invisible by EPR). Using this model, we can describe the dependence of the EPR intensity on the Ag doping. At low doping concentrations (<2 Ag/QD), Ag atoms are expected to act as n-type dopants.[33] As the concentration of Ag increases up to $\sim$ 2 Ag/QD, E_{F} shifts up in the energy gap and the amount of positively charged Se vacancies decreases; see Fig. 5(b). The result is a quenching of the signal at $g = 2.0045$. At Ag concentrations above 2 Ag/QD, Ag dopants are expected to behave as p-type dopants.[33] In this situation, E_{F} shifts down in energy; see Fig. 5(c). Thus, the amount of positively charged Se vacancies increases, which results in the increase of the intensity of the observed EPR signal. We note in Fig. 4 that the increase of EPR intensity observed for Ag concentrations above 2 Ag/QD is somewhat different for the two sample batches. We think that this difference may be related to a dispersion in the doping efficiency of the QDs, which is more significant for high Ag doping concentrations (>4 Ag/QD). Considering a random distribution of dopant atoms in the different QDs, we can see that for QD samples with low doping concentration (0 Ag/QD<[Ag]<2 Ag/QD), most QDs are n-type. For example, for a sample with an average of 1 dopant atom per QD, most QDs in the sample have 1 dopant, some (fewer) have 0 or 2 dopants, and only a very small amount will have 3 dopants and above. Thus, the majority of the QDs in the ensemble are n-type ([Ag]<2 Ag/QD) and a few are undoped. In contrast, in QD samples with high doping concentration (>4 Ag/QD) there is a broad mix of QDs with [Ag]< 2 Ag/QD (n-type) and [Ag]>2 Ag/QD (p-type). This leads to a complex situation where we have both n-type and p-type QDs contributing to the EPR signal intensity. Since we are at the cusp of switching from n-type to p-type QDs a small variation of the effective doping from batch to batch will have a large influence on the EPR signal intensity.

This difference may be related to an increase in the dispersion of doping efficiency of the QDs for higher Ag doping concentrations. We have a random distribution of dopant atoms in the different QDs comprising each sample. For QD samples with an average 1 dopant atom per QD, most QDs in the sample would have around 1 dopant, fewer would have 0 or 2, and the rest 3 and above. Thus, almost all the CdSe NCs would be either n-type doped or undoped. In contrast, in QD samples with an average 5-6 dopant atoms per QD, there will be a complex mix of both n-type and p-type doped QDs, which will give different averaged signals that might vary from batch to batch because we are at the cusp of switching from n- to p-type behavior.

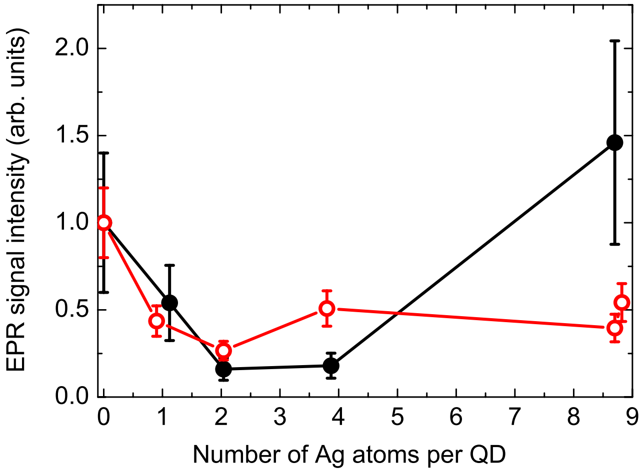

Figure 4: Intensity of the EPR signal at $g = 2.0045$ as a function of the number of Ag dopants per QD for two sample batches. For each batch, the EPR signal intensity is normalized to the intensity of the corresponding sample of undoped CdSe QDs.

Based on conductivity studies, the energy E_d of the transition from the neutral to the positive charge state of $\mathrm{V_{Se}}$ defects ($\mathrm{V_{Se}^{0/+}}$) in bulk CdSe has been estimated to be 150 meV below the semiconductor CB edge.[39] Further, the presence of $\mathrm{V_{Se}^{+}}$ defects has been suggested in CdSe QDs capped with a ZnSe shell.[15] These studies investigated the charge transport and the electroluminescence of diodes containing a layer of CdSe/ZnSe QDs with 6.8 nm in size. In these devices, the authors observed very low electron mobilities. They showed that this effect was due to electron trapping at defects in the QDs, which were present in a density of 8×10^{17} cm^{-3}.[15] From temperature-dependent current-voltage measurements they could estimate that the depth of the electron traps is ∼130 meV below the QDs CB. From comparison between this energy value and that estimated for the ionization energy of $\mathrm{V_{Se}}$ defects in bulk CdSe,[39] they suggested that the electron trapping states in their CdSe/ZnSe

QDs originate from $\mathrm{V}_{\mathrm{Se}}^{+}$ defects.

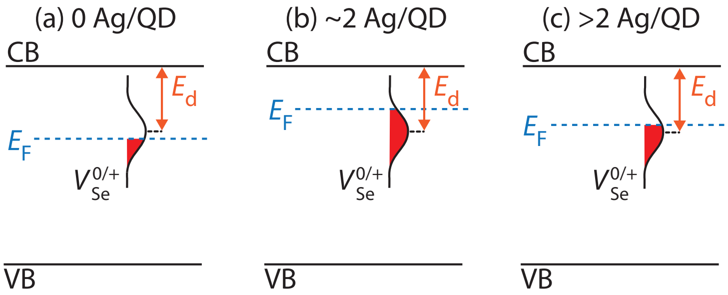

Figure 5: Scheme of the energy structure of ensembles of CdSe QDs with three Ag doping concentrations: (a) undoped, (b) ∼2 Ag/QD, and (c) >2 Ag/QD. In each scheme, the red area under E_F represents the amount of $\mathrm{V}_{\mathrm{Se}}^{0}$ defects in the QDs ensemble.

In Fig. 6, we show the dependence of the EPR signal at $g = 2.0045$ as a function of temperature T for samples of undoped CdSe QDs with two different mean sizes (2.7 nm and 5.4 nm). We see that in both cases the intensity of the EPR signal scales as T^{-1} between 30 K and room temperature, confirming that the EPR signal displays a Curie behavior within this temperature range. The observation of Curie behavior for temperatures at least up to room temperature shows that the population of these defects remains constant within this temperature range. Therefore, there is no thermal excitation of the paramagnetic defects up to room temperature. This enables us to infer a lower limit for the energy E_d. At 0 K, we have a certain density of neutral vacancy defects $n_{\mathrm{d},0}^{0}$. As T increases, neutral vacancies may be thermally excited to CB states and electrons populate CB states with a density n which is given by[42]

$$n^2 = \frac{N_\mathrm{c}}{2}\left(n_{\mathrm{d},0}^{0} - n\right) e^{-E_\mathrm{d}/k_\mathrm{B}T} \tag{1}$$

where $N_\mathrm{c} = \left(2\pi m_{\mathrm{CdSe}}^{*} k_\mathrm{B} T/h^2\right)^{3/2}$ is the effective density of CB states, $m_{\mathrm{CdSe}}^{*} = 0.13 m_0$ is the electron effective mass in bulk CdSe with m_0 being the free-electron mass,[39] k_B is the Boltzmann constant, and h is the Planck constant. The density of thermally excited $\mathrm{V}_{\mathrm{Se}}^{+}$ defects corresponds to n. The maximum of this density is $n_{\mathrm{d},0}^{0}$, i.e. when all neutral defects are thermally excited. The inset of figure 6 shows $P_{+} = n/n_{\mathrm{d},0}^{0}$, which corresponds to the fraction of thermally excited $\mathrm{V}_{\mathrm{Se}}^{+}$ defects, as a function of E_d and calculated for $T = 300$ K. In this figure, we see that the onset of P_+ occurs for $E_\mathrm{d} \approx 300$ meV. From this, we infer that the energy E_d is at least 300 meV. This low limit for E_d is higher than the previously reported value for the $\mathrm{V}_{\mathrm{Se}}^{0/+}$ energy level in bulk CdSe of 150 meV as described above.[39] The higher lower limit of E_d observed in the QDs may be due to the effect of confinement. For example, previous theoretical studies on P-doped Si QDs showed that confinement is expected to result in an increase of the dopant excitation energy with respect to that observed in the bulk counterpart with decreasing QD size.[43,44] The lower limit for E_d in our CdSe QDs is also higher than the excitation energy estimated in Ref. 15 for Se vacancy defects observed in CdSe/ZnS QDs with 6.8 nm in size. This difference may also be associated to a higher confinement in our CdSe QDs, which are smaller than the CdSe/ZnS QDs studied in Ref. 15.

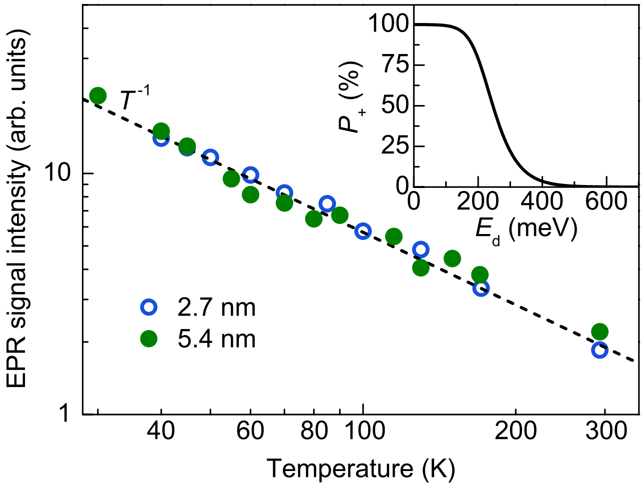

Figure 6: Temperature dependence of the intensity of the EPR signal at $g = 2.0045$ observed for undoped CdSe QDs with mean diameter of 2.7 nm (blue circles) and 5.4 nm (green dots). The dashed line represents a T^{-1} Curie behavior. The inset shows the dependence of the fraction of vacancy defects in their positive state P_+ as a function of the excitation energy of the defect E_d at room temperature.

Finally, we discuss the impact of the charge trapping defects observed in our study on the application of QDs in devices. In our CdSe QDs, the lowest measured density of trapping defects was $\sim 5 \times 10^{17}$ cm^{-3}, which corresponds to a sample of Ag-doped QDs. The densities of charge trapping defects in our samples were obtained directly from quantification of the intensity of the defects EPR spectrum. Other studies of the charge transport in films of CdSe QDs used current-voltage measurements to determine the trap density in these films, having estimated trap densities of about $2{\times}10^{16}$ cm^{-3}.[22] These values are very high in comparison to the defect densities necessary to achieve QD-based photovoltaics with efficiencies above 14%, in which the density of traps should be lower than 10^{12} cm^{-3}.[28] The lowest density of charge trapping defects observed in our CdSe QDs (5×10^{17} cm^{-3}) corresponds to having approximately 1 QD with a defect for every 50 QDs. From this value, we can estimate the order of magnitude of the distance l_{trap} that an electron in a film of QDs can move before it is captured by one of the charge trapping defects investigated here. If we assume that the electron travels between QDs in a straight line until it reaches a QD with a trapping defect, the distance l_{trap} is at most 100 nm. This value is in par with the distance $l_{\text{trap}}{\sim}80$ nm estimated for solar cells of PbS QDs with a power efficiency of 7%.[25] From this discussion, we confirm that the defects observed in our EPR study could have a performance-limiting effect on the electronic properties of devices based on CdSe QDs and that their reduction should have a significant impact on the improvement of the performance of these devices.

Conclusion

In this work, we report the observation of charge trapping defects in CdSe QDs using EPR, combined with electronic tuning of the QDs via chemically induced Ag doping. We observe that the intensity of the EPR signal due to defect traps depends on the concentration of electronic Ag dopants in the QDs, which provides supporting evidence for the mechanism of Ag doping of CdSe QDs suggested in previous studies.[33] Accordingly, Ag dopants are (interstitial) donors at concentrations up to ~2 Ag/QD and (substitutional) acceptors for higher Ag concentrations. Importantly, we show that the defects observed here act as charge traps, since the intensity of the EPR signal associated with these defects decreases by up to 80% with the incorporation of a few n-type Ag dopants per QD. From light-induced electron paramagnetic resonance, we further demonstrate that the defects studied in this work have a determinant role in pinning the Fermi energy in QD ensembles. We measure densities of charge trapping defects in the range of $10^{18} - 10^{20}$ cm^{-3}, which should be high enough to have a performance-limiting effect in devices based on these QDs.[28] From the characteristics of the EPR spectra we assign the trapping defects to positively charged Se vacancies.

Methods

CdSe QDs capped with tri-n-octylphosphine (TOP), tri-n-octylphosphine oxide (TOPO), hexadecylamine (HDA), and dodecylphosphonic acid (DDPA) were prepared via colloidal synthesis.[33] After synthesis, the QDs were washed to clean unreacted reagents from the dispersion. The QDs were isolated by precipitation with ethanol and redispersed in hexane or toluene.[33,45] Ag doping of the CdSe QDs was achieved by adapting a standard cation-exchange procedure for QDs.[33] In this procedure, as-synthesized intrinsic CdSe QDs were exposed to a solution of Ag cations and trioctylphosphine surfactants, which mediate the highly efficient incorporation of Ag dopants in the CdSe QDs. The entire synthesis of Ag-doped CdSe QDs was carried out under an inert atmosphere of N_2 to prevent their exposure to oxygen and water. In this study, we analyzed different batches of CdSe QDs samples doped with different concentrations of Ag dopants. The sample batches were produced independently from identical undoped CdSe QDs. All Ag concentrations mentioned in the this work were measured by inductively coupled plasma optical emission spectroscopy (ICP-OES). Using this technique, we deduced the net Ag:Cd:Se concentration and using the mean size of the QDs, we can evaluate the number of Cd and Se atoms per QD. Hence, we can deduce the average number of Ag atoms per QD. We should note that after Ag doping, numerous rounds of cleaning were performed to remove any Ag atoms that are not incorporated in the QDs and ensure that only those Ag atoms that were incorporated are detected with ICP-OES. Following this extensive cleaning, all the samples used in the

EPR measurements were analyzed for determining the Ag concentrations through ICP-OES regardless of what amount of Ag salt was added.

To characterize the size, shape, structure, composition, and optical properties of CdSe QDs, we used X-ray diffraction (XRD), transmission electron microscopy (TEM), and optical absorption spectroscopy. For XRD, a Bruker-AXS microdiffractometer was used to collect wide-angle powder patterns using the Cu-Kα line. Samples were prepared from concentrated dispersions of CdSe QDs in hexane. For TEM, an FEI Tecnai G2 F30 microscope was used to image the QDs with an acceleration voltage of 300 kV. Each sample was prepared by depositing a drop of a dilute dispersion of QDs in hexane onto a 400-mesh carbon-coated copper grid and allowing the solvent to evaporate at room temperature. The QD size distribution of each sample was extracted from the analysis of about 80 QDs observed in TEM images. Absorption spectra were obtained using a Cary 5E UV-Vis-near-infrared spectrophotometer.

Each sample of CdSe QDs used for EPR measurements was prepared by filling a few milligrams of dry QD powder into suprasil quartz tubes, which were then sealed under an inert atmosphere of N_2. The measurements were performed with a Bruker ESP 300E continuous-wave X-band spectrometer driven in absorption mode with a microwave frequency of $\nu = 9.38$ GHz. To perform low-temperature EPR, we used an Oxford Instruments ESR900 continuous-flow liquid He cryostat. We also performed photoexcited EPR measurements using a white light source (Thorlabs OSL1-EC) coupled to the spectrometer resonator and operating at a power of 150 W. Prior to measurement, each sample was kept inside the dark EPR resonant cavity for about 6 hours to prevent effects due to illumination by ambient light. After the measurement in the dark, the samples were illuminated for 45 minutes, after which the photoexcited measurements were performed. The density of charge trapping defects in our CdSe QD samples was determined via double numerical integration of the corresponding EPR signals and comparison with the signal intensity of a known spin standard consisting of a P-doped bulk crystalline Si. The intensity of all the EPR spectra shown in this work is normalized by the mass of the corresponding sample.

Acknowledgement

The authors thank Florian Ott from ETH Zurich for useful discussions. The authors acknowledge also the financial support of the FCT (Fundação para a Ciência e a Tecnologia, Portugal) via projects PTDC/FIS/112885/2009, PEst-C/CTM/LA0025/2013, and RECI/FIS-NAN/0183/2012 (FCOMP-01-0124-FEDER-027494) and of the Calouste Gulbenkian Foundation via the Research Stimulus Prize 2012. This work has been funded by FEDER funds through the COMPETE 2020 Programme and National Funds through FCT under the project UID/CTM/50025/2013 and by the Swiss National Science Foundation under Award No. 200021-140617. A. J. A. thanks FCT for a PhD fellowship (SFRH/BD/79223/2011).

References

1. Alivisatos, A. P. *Science* **1996**, *271*, 933.
2. Anthony, R.; Kortshagen, U. *Phys. Rev. B* **2009**, *80*, 115407.
3. Gupta, A.; Swihart, M. T.; Wiggers, H. *Adv. Funct. Mater.* **2009**, *19*, 696.
4. Kanemitsu, Y.; Okamoto, S.; Otobe, M.; Oda, S. *Phys. Rev. B* **1997**, *55*, R7375.
5. Luther, J. M.; Beard, M. C.; Song, Q.; Law, M.; Ellingson, R. J.; Nozik, A. J. *Nano Lett.* **2007**, *7*, 1779.
6. Nozik, A. J. *Nano Lett.* **2010**, *10*, 2735.
7. Beard, M. C.; Knutsen, K. P.; Yu, P.; Luther, J. M.; Song, Q.; Metzger, W. K.; Ellingson, R. J.; Nozik, A. J. *Nano Lett.* **2007**, *7*, 2506.
8. Coe-Sullivan, S. Nanotechnology for displays: a potential breakthrough for OLED displays and LCDs. SID Display Week 2012. 2012.

9. Hillhouse, H. W.; Beard, M. C. *Curr. Opin. Colloid Interface Sci.* **2009**, *14*, 245.

10. Sargent, E. H. *Adv. Mater.* **2008**, *20*, 3958.

11. Talapin, D. V.; Lee, J.-S.; Kovalenko, M. V.; Shevchenko, E. V. *Chem. Rev.* **2010**, *110*, 389.

12. Chuang, C. M.; Brown, P. R.; Bulović, V.; Bawendi, M. G. *Nature Mater.* **2014**, *13*, 796.

13. Kim, D. K.; Lai, Y.; Diroll, B. T.; Murray, C. B.; Kagan, C. R. *Nat. Comms.* **2012**, *3*, 1216.

14. Bozyigit, D.; Volk, S.; Yarema, O.; Wood, V. *Nano Lett.* **2013**, *13*, 5284.

15. Hikmet, R. A. M.; Talapin, D. V.; Weller, H. *J. Appl. Phys.* **2003**, *93*, 3509.

16. Katsiev, K.; Ip, A. H.; Fischer, A.; Tanabe, I.; Zhang, X.; Kirmani, A. R.; Voznyy, O.; Rollny, L. R.; Chou, K. W.; Thon, S. M. et al. *Adv. Mater.* **2014**, *26*, 937.

17. Kemp, K. W.; Wong, C. T. O.; Hoogland, S. H.; Sargent, E. H. *Appl. Phys. Lett.* **2013**, *103*, 211101.

18. Konstantanos, G.; Sargent, E. H. *Appl. Phys. Lett.* **2007**, *91*, 173505.

19. Kramer, I. J.; Sargent, E. H. *Chem. Rev.* **2014**, *114*, 863.

20. Talapin, D. V.; Rogach, A. L.; Kornowski, A.; Haase, M.; Weller, H. *Nano Lett.* **2001**, *1*, 207.

21. Zhitomirsky, D.; Kramer, I. J.; Labelle, A. J.; Fischer, A.; Debnath, R.; Pan, J.; Baker, O. M.; Sargent, E. H. *Nano Lett.* **2012**, *12*, 1007.

22. Ginger, D. S.; Greenham, N. C. *J. Appl. Phys.* **2000**, *87*, 1361.

23. Cordones, A. A.; Leone, S. R. *Chem. Soc. Rev.* **2013**, *42*, 3209.

24. Ip, A. H.; Thon, S. M.; Hoogland, S.; Voznyy, O.; Zhitomirsky, D.; Debnath, R.; Levina, L.; Rollny, L. R.; Carey, G. H.; Fischer, A. et al. *Nat. Nanotech.* **2012**, *7*, 577.

25. Zhitomirsky, D.; Voznyy, O.; Hoogland, S.; Sargent, E. H. *ACS Nano* **2013**, *7*, 5282.

26. Barkhouse, D. A. R.; Pattantyus-Abraham, A. G.; Levina, L.; Sargent, E. H. *ACS Nano* **2008**, *2*, 2356.

27. Stadler, P.; Sutherland, B. R.; Ren, Y.; Ning, Z.; Simchi, A.; Thon, S. M.; Hoogland, S.; Sargent, E. H. *ACS Nano* **2013**, *7*, 5757.

28. Kramer, I. J.; Sargent, E. H. *ACS Nano* **2011**, *5*, 8506.

29. Keeble, D. J.; Thomsen, E. A.; Stravinadis, A.; Samuel, I. D. W.; Smith, J. M.; Watt, A. A. R. *J. Phys. Chem. C* **2009**, *113*, 17306.

30. Voznyy, O.; Thon, S. M.; Ip, A. H.; Sargent, E. H. *J. Phys. Chem. Lett.* **2013**, 987.

31. Kim, D.; Kim, D.-H.; Lee, J.-H.; Grossman, J. C. *Phys. Rev. Lett.* **2013**, *110*, 196802.

32. Voznyy, O.; Sargent, E. H. *Phys. Rev. Lett.* **2014**, *112*, 157401.

33. Sahu, A.; Kang, M. S.; Kompch, A.; Notthoff, C.; Wills, A. W.; Deng, D.; M., W.; Frisbie, C. D.; Norris, D. J. *Nano Lett.* **2012**, *12*, 2587.

34. Cumberland, S. L.; Hanif, K. M.; Javier, A.; Khitrov, G. A.; Strouse, G. F.; Woessner, S. M.; Yun, C. S. *Chem. Mater.* **2002**, *14*, 1576.

35. Reiss, P.; Bleuse, J.; Pron, A. *Nano Lett.* **2002**, *2*, 781.

36. Schneider, J.; Rauber, A. *Solid State Commun.* **1967**, *5*, 779.

37. Meyer, B. K.; Omling, P.; Weigel, E.; Muller-Vogt, G. *Phys. Rev. B* **1992**, *46*, 15135.

38. Setzler, S. D.; Moldovan, M.; Yu, Z.; Meyers, T. H.; Giles, N. C.; Halliburton, L. E. *Appl. Phys. Lett.* **1997**, *70*, 2274.

39. *Landolt-Bornstein Numerical Data and Functional Relationships in Science and Technology, New Series*; New York, 16 April 2004.

40. Niesar, S.; Pereira, R. N.; Stegner, A. R.; Erhard, N.; Hoeb, M.; Baumer, A.; Wiggers, H.; Brandt, M. S.; Stutzmann, M. *Adv. Funct. Mater.* **2012**, *22*, 1190.

41. Kompch, A.; Sahu, A.; Notthoff, C.; Ott, F.; Norris, D. J.; Winterer, M. *J. Phys. Chem. C* **2015**, *119*, 18762.

42. Sapoval, H.; Hermann, C. *Physics of Semiconductors*, 1st ed.; Springer-Verlag, 1995.

43. Melnikov, D.; Chelikowsky, J. R. *Phys. Rev. Lett.* **2004**, *92*, 046802.

44. Chan, T. L.; Tiago, M. L.; Kaxiras, E.; Chelikowsky, J. R. *Nano Lett.* **2008**, *8*, 596.

45. Sahu, A.; Qi, L.; Kang, M. S.; Deng, D.; Norris, D. J. *J. Am. Chem. Soc.* **2011**, *133*, 6509.

Graphical TOC Entry